CROATICA CHEMICA ACTA CCACAA **71** (4) 949–974 (1998)

ISSN-0011-1643
CCA-2541 *Original Scientific Paper*

Adsorption of Nonspherical Particles at Solid/Liquid Interfaces

Zbigniew Adamczyk and Paweł Weroński*

Institute of Catalysis and Surface Chemistry, Polish Academy of Sciences
30-239 Cracow, ul. Niezapominajek 1, Poland

Received January 26, 1998; accepted April 21, 1998

Localized adsorption of nonspherical particles at solid/liquid interfaces was analyzed theoretically. Aproximate models for calculating interactions between particles and interfaces as well as between particles were discussed. It was demonstrated that for convex particles the Derjaguin model can be used for small separations, whereas for larger separations the equivalent sphere approach proved more appropriate. These analytical energy expressions were used in numerical Monte-Carlo RSA (random sequential adsorption) simulations of particle adsorption. Theoretical results concerning the blocking parameter (available surface function) and adsorption kinetics for short and long times were reported for prolate and oblate spheroids. Similarities and differences between flat (2D) and unoriented (quasi 3D) adsorption of particles were discussed and limiting power-law for the long-time regimes were specified. By extrapolation of the kinetic results the maximum (jamming) coverages for hard and interacting spheroids were determined. It was demonstrated that the jamming coverages under the conditions of unoriented adsorption exceed these of flat adsorption by many times for elongated objects. It was also demonstrated that the repulsive double-layer interactions decrease significantly the monolayer capacity of adsorbed layers of spheroidal particles. Implications of this phenomenon for protein adsorption were discussed.

This article is dedicated to Professor Egon Matijević on the occasion of his 75th birthday.

* Author to whom correspondence should be addressed.

INTRODUCTION

Adsorption of colloid and bioparticles at solid/liquid interfaces is of large practical significance in various practical processes involving separation steps, *e.g.,* filtration, ultrafiltration, electrophoresis, chromatography, *etc.* Learning about mechanisms and kinetics of these phenomena is also relevant for polymer and colloid science, biophysics and medicine enabling a better control of protein and cell separation, enzyme immobilization and prevention of thrombosis, biofouling of artificial organs *etc.*

It should be noted that the shape of most of surfactant molecules and bioparticles deviates from a spherical shape analyzed usually in various theoretical and experimental studies of adsorption kinetics. Various bacteria strains resemble elongated spheroids, *e.g.,* the *E. Coli* bacteria having the width to length ratio of about 0.5[1] or the bacteria from the *Actinomyces* group characterized by a much larger elongation.[2]

Similarly, the shape of important globular proteins like bovine serum albumin (BSA) or fibrinogen[3–6] resembles prolate spheroids with the axis ratio about 0.28 and 0.2–0.18, respectively. The same concerns the *tobacco mosaic* virus having almost perfectly cylindrical shape.[7]

Other examples of highly anisotropic particles are the red blood cells, blood platelets, pigments and synthetic inorganic colloids: gold, silver iodide, silver bromide, barium sulphate *etc.*[8,9] The entire variety of nonspherical particles has been synthesised over decades in the well-known school of Matijević.[10–15] Also, model polymeric colloid system of nonspherical mono-disperse particles, *e.g.,* PTFE or polystyrene latexes[16] or silica covered bohemite[17] can now be prepared in a reproducible way.

Adsorption kinetics of these particles was usually interpreted in terms of the Langmuir model developed originally for gas adsorption.[18] The surface blocking parameter B (which should be more appropriately referred to as the available surface function) was assumed to be in the form $1 - \theta/\theta_s$ (where θ_s is the empirically determined maximum surface coverage). Although the validity of the Langmuir model for adsorption from liquid phases over continuous surfaces seems doubtful[19] it was quite often used in the literature for interpreting adsorption of proteins,[20–22] colloids,[23–27] and bacteria.[28,29] As discussed at length in Ref. 19 this seems justified for low surface coverage only.

A more realistic theoretical determination of B for colloidal particles can be achieved using the recent theoretical models, especially various mutations of the random sequential adsorption (RSA) approach.[30–34]

Despite the simplicity of the underlying assumptions the topology of particle distributions generated in RSA processes becomes complex for higher

surface concentrations, so a proper description of the RSA process for spherical particles in 2D was achieved in terms of the Monte-Carlo type computer simulations.[19,31–36]

For nonspherical particles the RSA simulations become even more complicated, especially in the case of interacting particles. However, in recent years a considerable progress in this field has been achieved and many interesting theoretical results were reported concerning both the kinetic aspects and structure of the adsorbed layer of nonspherical particles. Thus, the goal of this paper was to critically review these works and show possible ways of using these results for interpretation of experimental data concerning protein adsorption. We concentrate on adsorption from suspensions kinetically stabilized by the presence of repulsive double-layer electrostatic interactions. Hence, the dispersion and other type interactions between particles will be neglected. On the other hand, the interface should be treated as a perfectly sticking plane, in the sense, that every particle touching it will make a permanent contact losing its possibility to move laterally (localized adsorption postulate).

INTERACTIONS OF NONSPHERICAL PARTICLES

An exact determination of interaction energy of nonspherical particles in the general case seems prohibitive due to the inherent many-body problem and the lack of appropriate coordinate system for expressing the Poisson-Boltzmann equation governing the electrostatic potential distribution. However, by observing that particle and protein adsorption takes usually place from concentrated electrolyte solutions one can treat the electrostatic interactions as short-ranged (in comparison with particle dimensions). This enables one to get rid of the many-body problem by exploiting the additivity rule and calculating the interparticle energy as sum of contributions stemming from particle pairs. Even if the problem is effectively reduced to a two-particle interactions it cannot be solved in any exact form. Approximate methods are available only, such as the generalized Derjaguin method[37,38] and the equivalent sphere approach (ESA) developed recently.[39,40]

According to the original Derjaguin method the interactions of spheres were calculated as a sum (integral) of corresponding interactions of infinitesimal surface elements having a planar geometry. Later on this approach was extended to unequal spheres and convex particles of arbitrary shape.[37,38] The great advantage of the Derjaguin method is that it enables one to calculate interactions between bodies of complicated geometry (cylinders, spheroids) in terms of the well studied case of two-plate interactions. The

appropriate expressions for the interaction force F and energy ϕ assume the form

$$F = 2\pi G_D \int_{h_m}^{\infty} \Delta\Pi(h)\, dh$$
$$\phi = 2\pi G_D \int_{h_m}^{\infty} \Phi(h)\, dh \tag{1}$$

where $\Delta\Pi$ is the pressure between flat plates (force per unit area), Φ is the interaction energy per unit area of the plates, h is the distance between plates, h_m is the minimum separation between plates (particles) and G_D is the geometrical Derjaguin factor given by the expression

$$G_D = \sqrt{\frac{R_1' R_1'' R_2' R_2''}{(R_1' + R_2')(R_1'' + R_2'') + (R_1'' - R_1')(R_2'' - R_2')\sin^2\varphi}} \tag{2}$$

where R_1', R_1'', R_2', R_2'' are the four principal radii of curvature of the interacting particles to be evaluated at the point of minimum separation and φ is the angle between principal planes normal to particle surfaces at the point of minimum separation.

When particles adsorb flat, $\varphi = 0$, and Eq. (2) simplifies to the form derived previously.[38,39]

$$G_D = \sqrt{\frac{R_1' R_1'' R_2' R_2''}{(R_1' + R_2')(R_1'' + R_2'')}} \tag{3}$$

For unequal spheres when $R_1' = R_1'' = a_1$ and $R_2' = R_2'' = a_2$ Eq. (3) gives $G_D = a_1 a_2 / (a_1 + a_2)$; for equal spheres $G_D = 0.5\, a$, *i.e.,* two times smaller than for the sphere/plane interactions when $G_D = a$.

However, for convex bodies an exact evaluation of the factor G_D is difficult and can only be done numerically.[39] Some useful analytical approximations can be derived for limiting orientations of two spheroids, *i.e.,* parallel, perpendicular, edge to edge and one over another.

As discussed,[39,40] according to the Derjaguin model, the interactions between prolate spheroids may differ by many times (for elongated objects) when particle orientation is changed from parallel to perpendicular. This seems to have considerable applications for adsorption of elongated interacting particles (*e.g.*, proteins).

Using Eq. (1) one can derive useful expressions for interaction energy of nonspherical particle from the known results for plane geometry. Thus, in the low potential limit (linearized Poisson-Boltzmann equation describing electrostatic field distribution between plates) the appropriate equation for energy takes the form[41]

$$\phi = G_{\mathrm{D}}\,\varepsilon\left(\frac{kT}{2e}\right)^2\left[\left|\pm\left(\bar{\psi}_1^{0^2}+\bar{\psi}_2^{0^2}\right)\ln(1-\mathrm{e}^{-2\kappa h_{\mathrm{m}}})+2\bar{\psi}_1^{0}\bar{\psi}_2^{0}\ln\left(\frac{1+\mathrm{e}^{-\kappa h_{\mathrm{m}}}}{1-\mathrm{e}^{-\kappa h_{\mathrm{m}}}}\right)\right]\right| \quad (4)$$

where $\bar{\psi}_1^{0}$ and $\bar{\psi}_2^{0}$ are the dimensionless surface potentials of the two particles involved, $\kappa^{-1} = Le = (\varepsilon kT / 8\pi e^2 I)^{1/2}$ is the Debye screening length, ε is the dielectric constant of the medium, k is the Boltzmann constant, T is the absolute temperature, e the elementary charge and I the ionic strength of the electrolyte solution, the upper and lower signs denotes the constant charge and constant potential models, respectively.

For equal potentials (but not necessarily particle sizes) Eq. (4) simplifies to the original Derjaguin formula when $G_{\mathrm{D}} = a_1\,a_2 / (a_1 + a_2)$ is substituted, *i.e.*,

$$\phi = \frac{a_1 a_2}{a_1 + a_2}\varepsilon\left(\frac{kT}{e}\right)^2\bar{\psi}^{0^2}\ln\left[1+\mathrm{e}^{-\kappa h_{\mathrm{m}}}\right] \quad (5)$$

On the other hand, for arbitrary high potentials (nonlinear double-layer model) one can derive from the Derjaguin model the following expression for particle interaction at larger distances

$$\phi = G_{\mathrm{D}}\,\varepsilon\left(\frac{kT}{e}\right)^2 Y_1^{0}Y_2^{0}\mathrm{e}^{-\kappa h_{\mathrm{m}}} \quad (6)$$

where Y_1^0, Y_2^0 are the effective surface potentials which can well be approximated for a 1–1 electrolyte by $Y_1^0 = 4\mathrm{th}\left(\bar{\psi}_1^0 / 4\right)$. For other electrolytes and electrolyte mixtures Y^0 can only be evaluated numerically.[40]

It should be noted, however, that the Derjaguin model gives reasonable estimates of interactions for short distances and large particles only when the inequalities $\kappa R >> 1$ and $\kappa h_{\mathrm{m}} >> 1$ are met simultaneously. For larger distances the Derjaguin model tends to overestimate the interactions giving also wrong asymptotic dependencies for ϕ. This has been demonstrated by performing exact numerical simulations for dissimilar sphere interactions.[42] Although analogous calculations for spheroids cannot be carried out, one

may conclude that the Derjaguin model does not reflect properly spheroid interactions at large distances.

Therefore, for larger separations other approximate models were developed like the equivalent sphere approach (ESA) discussed in Refs. 39, 40. The essence of this model consist in replacing the interactions of convex bodies by analogous interactions of spheres having properly defined radii of curvature. As postulated,[39] these radii should be calculated as the following means of the principal radii of curvature evaluated at the point of minimum separtion between the bodies involved, *i.e.,*

$$R_1 = \frac{2R_1' R_1''}{R_1' + R_1''}$$
$$R_2 = \frac{2R_2' R_2''}{R_2' + R_2''} \tag{7}$$

The advantage of the ESA consist in the fact that many known numerical and analytical results concerning sphere interactions can directly be transferred to spheroidal particles. Thus, for example, the commonly used expression derived for two spheres by accepting the linear superposition approach (LSA)[43] can be generalized for spheroidal particles to the form

$$\phi = \varepsilon \left(\frac{kT}{e}\right)^2 Y_1^0 Y_2^0 \frac{R_1 R_2}{R_1 + R_2 + h_m} e^{-\kappa h_m} = \phi_0 \frac{\overline{G}_e^0}{1 + \overline{G}_e \frac{h_m}{a}} e^{-\kappa h_m} \tag{8}$$

where

$$\phi_0 = \varepsilon a \left(\frac{kT}{e}\right)^2 Y_1^0 Y_2^0$$

a is the spheroid semi-axis and

$$\overline{G}_e^0 = \frac{R_1 R_2}{a(R_1 + R_2)} = \frac{2R_1' R_1'' R_2' R_2''}{a\left[R_1' R_1'' (R_2' + R_2'') + R_2' R_2'' (R_1' + R_1'')\right]}$$
$$\overline{G}_e = \frac{a}{(R_1 + R_2)} = \frac{a(R_1' + R_1'')(R_2' + R_2'')}{2\left[R_1' R_1'' (R_2' + R_2'') + R_2' R_2'' (R_1' + R_1'')\right]} \tag{9}$$

are the two geometrical correction factors.

As can be noted, Eq. (8) describes the exponetially decaying Yukawa-type potential, used widely in statistical mechaniscs. Due to its simple mathematical shape Eq. (8) was also extensively exploited in numerical simulations of nonspherical particle adsorption. However, analogously as for the Derjaguin model, the correction factors $\overline{G}_e^0$ and $\overline{G}_e$ can be evaluated analytically for some limiting orientations only. For intermediate orientation one has to use numerical method to calculate the equivalent radii of curvature.[39,40]

Another approximation which can be used for describing electrostatic interactions of nonspherical particles in the case of large κa values is based on the effective hard particle (EHP) concept introduced originally by Barker and Henderson.[44] According to this method the true interaction potential between particles is replaced by the hard wall potential. Physically this means that the interacting particles can be treated as hard ones having the equivalent dimensions increased over the true geometrical dimensions by the small value h^* (skin), which can be treated as the effective interaction range. It can be shown by performing numerical simulations discussed below that h^* is proportional to the $(\kappa a)^{-1}$ parameter.

THEORETICAL PREDICTIONS

General Considerations

Localized adsorption of nonspherical particles was usually described in terms of the above mentioned RSA model whose underlying assumptions are:

(i) particle adsorption occurs at a microscopically homogeneous interface, *i.e.,* the probability density of choosing a given particle position and orientation is uniform,

(ii) adsorbed particles cannot overlap with each other; additionally in the case of interacting particles the probability of adsorption in the vicinity of preadsorbed particles is modified according to the Boltzmann distribution;

(iii) after adsorption particle positions and orientations remain time-independent, *i.e.,* adsorption is postulated localized and irreversible.

Using the RSA approach extensive simulations of adsorption kinetics and jamming concentrations were performed for such particle shapes as cubes and cylinders,[45–47] spherocylinders and spheroids.[48,49] All these results were derived by assuming a flat (side on) orientation of the adsorbing particles only. The case of arbitrary spheroid orientation (unoriented quasi 3-dimensional 3D adsorption) was treated for noniteracting[50] and interacting[51] particles.

The advantage of the RSA approach is not only that it allows one to perform complex numerical simulations but also to formulate some limiting laws for low and high coverage adsorption regimes. Thus, for not too high coverages, the surface blocking parameter B can be expressed in terms of the power series expansion of θ, *i.e.*,[50]

$$B(\theta) = 1 - C_1\,\theta + C_2\,\theta^2 - C_3\,\theta^3 + \cdots C_n\,\theta^n \tag{10}$$

The expansion coefficients $C_1 \div C_n$, directly related to the virial coefficients, were determined up to the order of three for the side-on adsorption of noninteracting spheroids, cylinders and spherocylinders.[48] Additionally, for arbitrary convex body the C_1 coefficient can be expressed analytically[52] in the form

$$C_1 = 2 + \frac{P^2}{2\pi S_g} \tag{11}$$

where P is the perimeter of the particle and S_g its geometrical cross-section. For spheroids P is given by the complete elliptic integral of the second kind and cannot be evaluated explicitly. However, a simple interpolating formula for C_1 was given[39]

$$C_1 = \frac{4(\pi^2 - 4)}{\pi^2} + \frac{8}{\pi^2}\left(A + \frac{1}{A}\right) \tag{12}$$

where $A = b/a$, b and a are the shorter and longer semiaxes, respectively.

For interacting particles the C_1 coefficient can only be evaluated numerically.[39,50] These numerical results were approximated the following interpolating expression for the side-on adsorption of spheroids[39]

$$C_1^* = C_1 + 4\left(1 + \frac{1}{A}\right)H^* + \frac{4}{A}H^{*2} \tag{13}$$

For the unoriented adsorption of prolate and oblate spheroids one has accordingly Ref. 50

$$C_1^* = (2.07 + 0.811A^* + 2.37A^{*2} - 1.25A^{*3})(1 + H^*)\left(1 + \frac{H^*}{A}\right)$$

$$C_1^* = (1.59 + 2.80A^* - 0.388A^{*2})(1 + H^*)^2 \tag{14}$$

$$A^* = \frac{A + H^*}{1 + H^*}$$

The effective interaction range $H^* = h^*/a$ occurring in these expressions is proportional for thin double layers to the $Le = \kappa^{-1}$ parameter. This can be observed in Figure 1 where the dependence of H^* on κa is shown for unoriented adsorption of interacting prolate spheroids characterized by various elongation parameter A and the interaction potential given by Eq. (8). Thus, the dependence of H^* on κa becomes

$$H^* = (\kappa a)^{-1}\ \xi \tag{15}$$

with the proportionality constant $\xi = 1/2 \ln (\phi_0/\phi_{ch})$ and ϕ_{ch} being the characteristic energy close to one kT unit.[39,50]

As can be deduced from Eqs. (12–14) the value of the C_1 constant increases considerably for elongated spheroids when the H^* value becomes significant. According to Eq. (10) this should exert a profound influence on

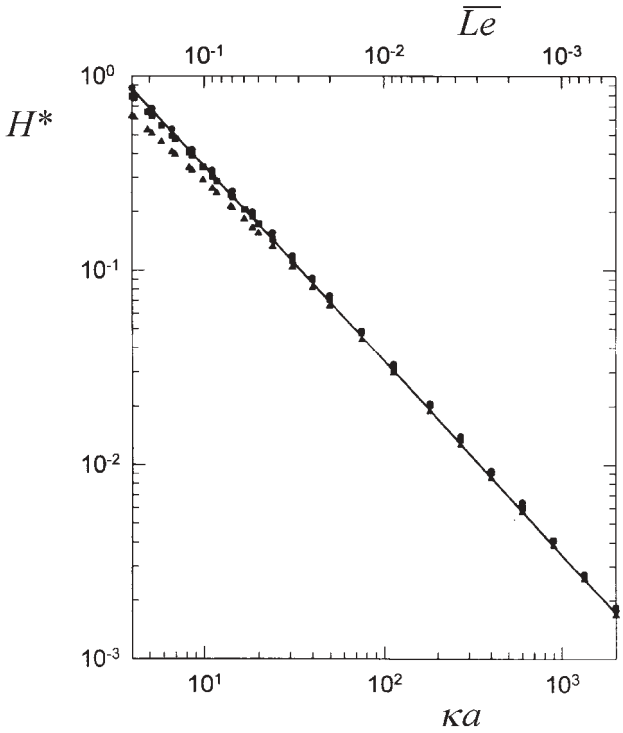

Figure 1. The dependence of the effective interaction range H^* on the κa (Le) parameter. The points represent exact numerical results for prolate spheroids characterized by various alongation: (●) $A = 1$ (spheres), (■) $A = 0.5$, (▲) $A = 0.2$; the solid lines show the analytical approximation calculated from the equation $H^* = 0.5\ \overline{Le} \ln (\phi_0 / \phi_{ch})$.

particle adsorption since the C_1 constant determines the most significant (leading) term of this series expansion. Moreover, it has been shown[50] that the C_2 constant of the series expansion Eq. (10) is connected with C_1 through by the simple dependence

$$C_2 = f C_1^2 \tag{16}$$

where the proportionality constant f was found equal 0.295 for A = 0.2 (elongated spheroids).

Using these results one can derive analytical expressions for particle adsorption kinetics considering that according to definition one has[50,51]

$$\frac{\mathrm{d}\theta}{\mathrm{d}\tau} = B(\theta) \tag{17}$$

where $\tau = t / t_{\mathrm{ch}}$ is the dimensionless adsorption time (t_{ch} is the characteristic adsorption time defined usually as the time of forming a random monolayer).[50,51] By substituting the expansion Eq. (10) (containing the leading term only) into Eq. (17) and performing the necessary integration one obtains the simple expression

$$\theta = \theta_{\mathrm{s}} \left(1 - \mathrm{e}^{-\frac{1}{\theta_{\mathrm{s}}}\tau} \right) \tag{18}$$

where θ_{s} is the saturation coverage equal to $\dfrac{1}{C_1}$.

This expression is formally equivalent to that derived by accepting the Langmuir model of particle adsorption.[19–25] It should be stressed however, that it can only be used for initial stages of particle adsorption and never for estimating the maximum coverage attained for large times as usually done in the literature.

On the other hand, using the two terms in the series expansion Eq. (10) one can derive the improved kinetic equation[50–51]

$$\theta = \theta_1 \frac{1 - \mathrm{e}^{-pC_1\tau}}{1 - \dfrac{\theta_1}{\theta_2}\mathrm{e}^{-pC_1\tau}} \tag{19}$$

$$\theta_1 = \frac{C_1}{2C_2}(1-p), \quad \theta_2 = \frac{C_1}{2C_2}(1+p), \quad p = \left(1 - \frac{4C_2}{C_1^2}\right)^{1/2}$$

When $4C_2 / C_1^2 > 1$ the solution is[50]

$$\theta = \frac{2\mathrm{tg}\left(\frac{1}{2}C_1 p\tau\right)}{C_1 p\left|\left[1+\frac{1}{p}\mathrm{tg}\left(\frac{1}{2}C_1 p\tau\right)\right]\right|}, \quad p = \left(\frac{4C_2}{C_1^2}-1\right)^{1/2} \tag{20}$$

Eqs. (19–20) are supposed to approximate well adsorption kinetics of nonspherical particles for a much wider range of coverages than Eq. (18).

Numerical Simulations

In the general case of arbitrary surface concentration of particles the blocking parameter $B(\theta)$ and adsorption kinetics were calculated according to the simulation method described in literature.[39,50,51] The algorithm consisted from three main calculation modules repeated in a loop:

(i) The virtual (adsorbing) spheroidal particle was generated having the position vector $\boldsymbol{r}_v$ and the orientation vector $\hat{\boldsymbol{e}}$ (*cf.* Figure 2); the size of the square simulation plane ΔS was normalized to unity and the relative cross-section surface area of the virtual particle S_g with respect to ΔS was usually 2×10^{-4}. At the perimeter of the simulation plane the periodic boundary conditions were applied

(ii) then, overlapping test was performed by scanning the adsorbing particle vicinity and using the Veillard-Baron[53] function. If overlapping occurred than the step (i) was repeated, otherwise the minimum surface to surface distances between the virtual and previously adsorbed particles were determined by the procedure described in Ref. 39. Knowing the dis-

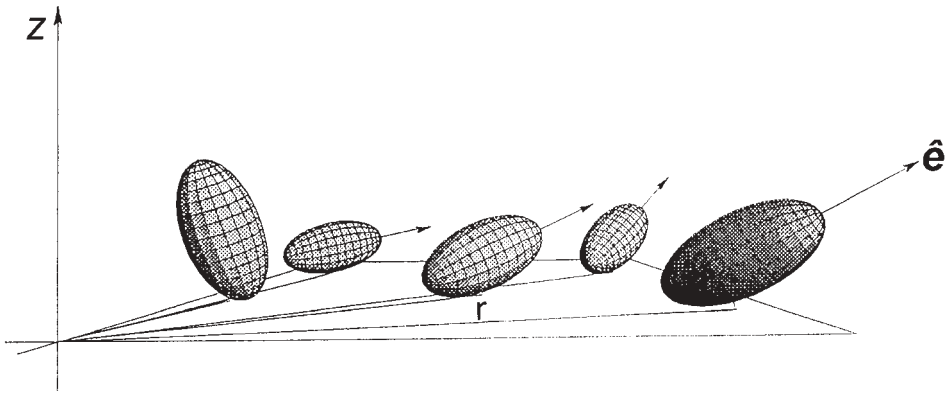

Figure 2. A schematic representation of quasi 3D random sequential adsorption of spheroidal particles at a planar interface.

tances the net interaction energy was calculated as a sum of pair interactions using Eq. (8)

(iii) finally, the virtual particle was adsorbed with the probability δp given by the Boltzmann relationship. After adsorption the coordinates and orientation of the particle remained unchanged.

The blocking parameter B was calculated using the method described by Schaaf and Talbot.[32,33] According to their procedure the RSA process was continued until a desired surface concentration was attained. Then, a large number of trials N_t of placing a new particle was performed by keeping the surface concentration constant. The number of successful attempts (would be adsorption events) was found to be N_{succ}. Taking advantage of the general large number probability law the blocking parameter $B(\theta)$ was calculated as the limit of the ratio N_{succ} / N_t for $N_t \to \infty$.

On the other hand, particle adsorption kinetics was simulated directly by monitoring the number of successful adsorption events as a function of the dimensionless time τ defined as[19]

$$\tau = \frac{t}{t_{ch}} = \frac{N_{att}}{N_{ch}} = \frac{N_{att}}{\left(\frac{1}{\overline{S}_g}\right)} \tag{21}$$

where N_{att} is the overall number of attempts at placing particles (repetitions of the simulation loop) and N_{ch} is the characteristic number of particles.

Using the above simulation scheme extensive calculations of $B(\theta)$ were performed for interacting spheroidal particles of prolate and oblate shape both for side-on[39] and unoriented adsorption.[50,51] The influence of the elongation parameter A and the κa parameter (H^*) on $B(\theta)$ was systematically studied. Some selected results of these calculations are shown in Figure 3 for the side-on adsorption and in Figure 4 for the unoriented adsorption (A = 0.2). As can be seen in both cases the analytical approximation Eq. (10) (containing the terms up to the order of two) describes reasonably well the exact numerical results for low and moderate range if surface coverages θ. It should also be noted that the increase in the H^* parameter (which according to Eq. (15)) is proportional to Le) was resulting in a significant decrease of B for the same surface coverage θ*., i.e.,* the blocking effects became more pronounced when H^* increases. Thus, for H^* = 0.2 the blocking parameter decreased to negligible values already for θ as low as 0.2.

A similar trend was observed for unoriented adsorption (see Figure 4), *i.e.*, the increase in H^* resulted in a significant decrease in the blocking parameter $B(\theta)$. It should be noted, however, that in comparison with the side-on adsorption, the coverages attained under the unoriented adsorption

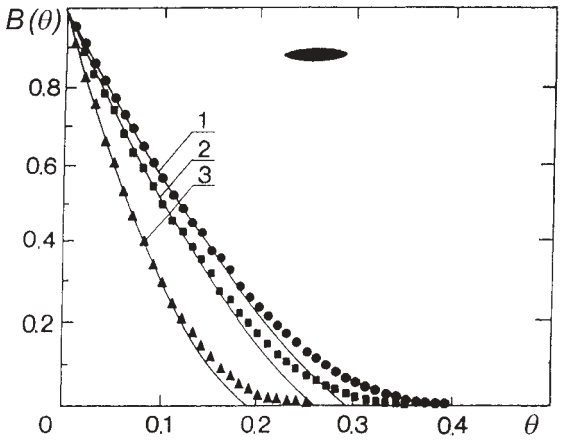

Figure 3. The dependence of B on θ for interacting prolate spheroids (A = 0.2), side-on adsorption. The points denote the numerical simulations performed for: (1) H^* = 0 (hard particles), (2) H^* = 0.1, (3) H^* = 0.2; the continuous lines denote the analytical results calculated from Eqs. (10–15).

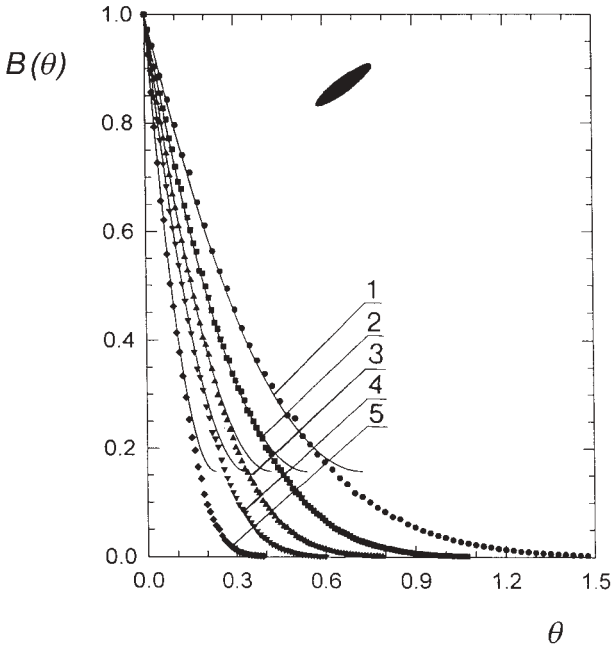

Figure 4. The dependence of B on θ for interacting prolate spheroids (A = 0.2), unoriented adsorption. The points denote the numerical simulations performed for: (1) H^* = 0 (hard particles), (2) H^* = 0.05, (3) H^* = 0.1, (4) H^* = 0.15, (5) H^* = 0.25; the continuous lines denote the analytical results calculated from Eqs. (10–15).

regime were much higher which is a direct manifestation of the fact that many more particles can be »jammed« in the monolayer under orientation close to perpendicular. It can also be deduced when comparying results shown in Figures 3–4 that the $B(\theta)$ function for interacting particles under conditions of unoriented adsorption may resemble very closely adsorption of hard (noninteracting) particles under the side-on adsorption regime.

Kinetics of Particle Adsorption

Using the above RSA simulation scheme one can determine not only the $B(\theta)$ function but also generate kinetic runs, *i.e.,* the θ *vs.* τ dependencies which are of primary interest from practical viewpoint. Therefore, extensive simulations were performed to determine adsorption kinetics both for the side-on[39] and unoriented adsorption regime.[50,51] Some characteristic results illustrating the difference between side-on and unoriented adsorption of prolate spheroids are shown in Figure 5a for shorter adsorption times ($\tau < 5$). The exact numerical results are compared with the analytical results stemming from the quasi-Langmuir model (Eq. 18) and from Eqs. (19–20). As can be noted, the Langmuir model can be used for short adsorption times only, *i.e.*, for $\tau < 1$, whereas the improved analytical model, described by Eqs. (19–20) seems applicable for much wider time interval. It can also be noticed from the kinetic data shown in Figure 5a that the amount of particles adsorbed after a given time under the 3D (unoriented) regime is almost four times larger than for the side-on adsorption. As mentioned above, this effect should have profound significance for proteins characterized by elongated molecule shape (*e.g.*, fibrinogen).

It should be mentioned, however, that due to the considerable decrease in particle adsorption rate for longer adsorption times (which is characteristic for all RSA processes) the kinetic curves like these shown in Figure 5a cannot be effectively presented using the natural coordinate system θ *vs.* τ. Topological considerations and extensive numerical simulations[48,50,51] suggest that the asymptotic adsorption kinetics of nonspherical particles for long times should be described, in analogy as for spheres, by the power-law dependence, *i.e.*,

$$\theta_\infty - \theta = K\tau^{-\frac{1}{m}} \tag{22}$$

where θ_∞ is the jamming concentration of adsorbed particles, K is the proportionality constant and m is the natural number equal 3 for side-on adsorption and 4 for unoriented adsorption (in the case of spheres $m = 2$).

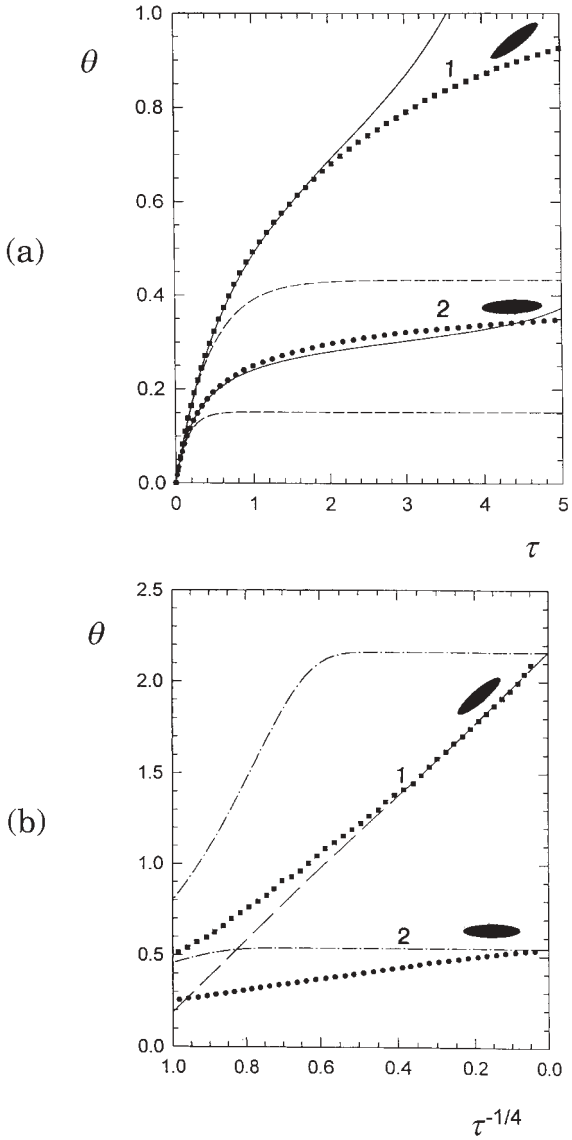

Figure 5. Part (a). Adsorption kinetics of prolate spheroids $A = 0.2$, $H^* = 0$ (hard particles). The dependence of θ on the dimensionless adsorption time τ determined numerically (points) for the unoriented (upper part) and side-on adsorption regime; the solid lines denote the analytical results calculated from Eqs. (19–20) and the broken lines denote the results stemming from the Langmuir model, Eq. (18) with $\theta_s = 1/C_1$. Part (b). Adsorption kinetics for long times expressed as θ *vs.* $\tau^{-1/4}$ determined numerically (points); the dashed line denotes the fitting functions calculated from Eq. (22) and the dash-dot lines denote the results calculated from the modified Langmuir model, Eq. (18) with $\theta_s = \theta_\infty$.

Eq. (22) suggests that the use of the θ *vs.* $\tau^{-1/4}$ coordinate system should be more appropriate for expressing the kinetic data for $\tau >> 1$. This transformation has an additional advantage of compressing the infinite τ domain into a finite one. Such plot derived from numerical simulations performed for hard prolate spheroids (A = 0.2) is shown in Figure 5b. As can be observed, by using this transformation, the kinetic data can indeed be expressed as linear dependence of θ on $\tau^{-1/4}$ for a broad range of τ in the case of unoriented adsorption (the analogous plot for side-on adsorption becomes nonlinear due to different exponent). For comparison, the results stemming from the widely used Langmuir model (Eq. 18) are also shown in Figure 5b. It should be mentioned that in this case, unlike Figure 5a where $\theta_s = 1/C_1$, the θ_s values were chosen to match numerical simulations for $\tau \to \infty$. As can be seen the character of the curves stemming from the Langmuir model deviates significantly from the numerical predictions characterized well by the power-law dependence. It seems, therefore, that the RSA model predicting a long-lasting approach to the saturation (jamming) coverages can better account for experimental data concerning protein adsorption[54] which were interpreted in terms of two different adsorption regimes widely differing in rate.

The existence of the above mentioned linear regime enabled one to determine very accurately the jamming (saturation) values of θ_∞ by extrapolating the θ *vs.* $\tau^{-1/4}$ dependencies generated for long adsorption times. The θ_∞ values for hard particles are quantities of considerable practical interest since they determine the maximum capacity of a monolayer formed in localized adsorption processes in the limit of high ionic strength. The extrapolation procedure is necessary because a direct determination of θ_∞ is not feasible due to the limited value of the computer accessible τ values equal to about 10^5 at the most. The monolayers formed after such adsorption time by prolate and oblate spheroids (A = 0.2) are shown in Figure 6.

The dependence of θ_∞ on A determined by the extrapolation procedure for hard prolate spheroids[50] is shown in Figure 7a. The points denote the numerical simulations and the solid line represents the fitting function given by

$$\theta_\infty = 0.304 - 0.123A + \frac{0.365}{A} \tag{23}$$

As one can see in Figure 7a the numerical results, reflected well by Eq. (23), lie above the values calculated as an average of the side-on and perpendicular orientations (shown by the broken line). This suggests that orientations close to perpendicular are preferred in adsorption of elongated

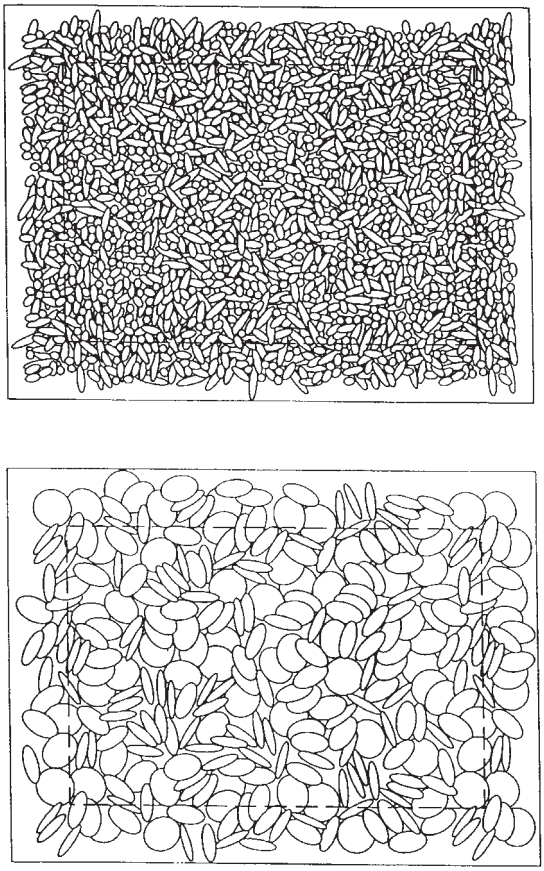

Figure 6. A top view of the »monolayers« of adsorbed spheroidal particles, generated in RSA simulations; upper part – prolate spheroids A = 0.2 (θ = 2.1), lower part – oblate spheroids A = 0.2 (θ = 1.95).

spheroids (this can also be deduced qualitatively from the view of the monolayer shown in Figure 6).

Analogous dependence of θ_∞ on A calculated numerically for hard oblate spheroids[50] is shown in Figure 7b together with the fitting function

$$\theta_\infty = 0.768 - 0.473A + \frac{0.251}{A} \tag{24}$$

As can be observed in Figure 7b, analogously as for prolate spheroids, the exact data exceed the values calculated as average of side-on and perpendicular orientations.

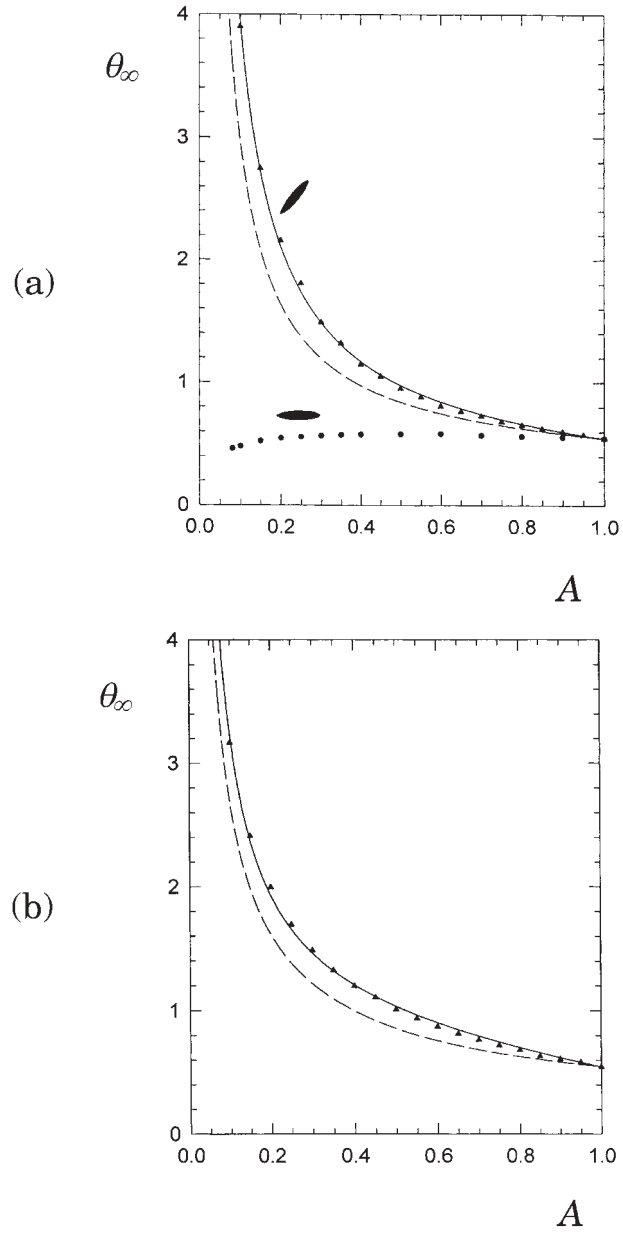

Figure 7. Part (a). The dependence of the jamming (maximum) surface coverage θ_∞ on the elongation parameter A determined numerically (points) for hard prolate spheroids under unoriented and side-on adsorption conditions; the solid line denotes the interpolation results calculated from Eq. (23) and the broken line shows the averaged results. Part (b). Same as for (a) but for oblate spheroids; the solid line was calculated from Eq. (24).

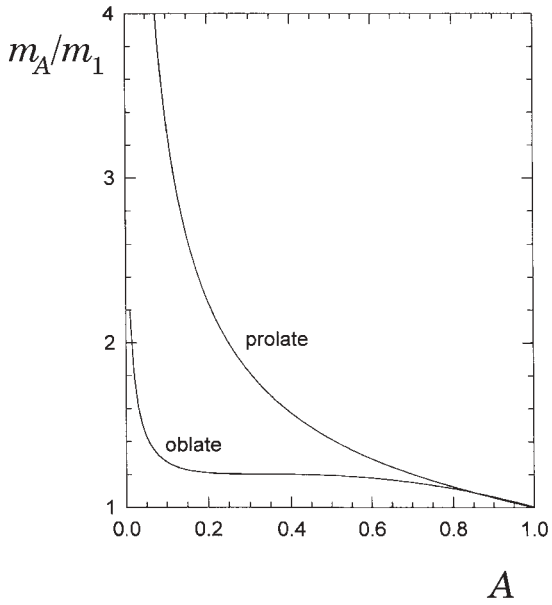

Figure 8. The dependence of the normalized monolayer mass m_A / m_1 on the A parameter determined numerically for prolate and oblate spheroids.

The data shown in Figures 7a–7b can also be used for determining the effect of shape change of adsorbing particles when its volume or molecular mass remains constant. Such graphs are shown in Figure 8, both for prolate and oblate spheroids, in the form of the dependence of m_A / m_1 on the A parameter (where m_A is the mass of the adsorbed monolayer per unit area and m_1 is the mass of monolayer of spherical particles). As one can observe in Figure 8 changing the shape of a particle to more elongated $A \to 0$ (at fixed molecular mass) resulted in a considerable increase in the mass of the monolayer. This can be expressed in the limit when $A \to 0$ as $m_A / m_1 \to 0.668\, A^{-2/3}$. In the case of oblate spheroids, this effect is much less pronounced since $m_A / m_1 \to 0.46\, A^{-1/3}$ in the limit of $A \to 0$.

The above discussed results concerned hard particles only and can be treated as the upper estimate of monolayer densities in the limit when the interaction range H^* tends to zero.

The effect of interactions on kinetics of prolate spheroid adsorption (A = 0.2, unoriented regime) is shown in Figure 9a for shorter times ($\tau < 5$) and in Figure 9b for longer times. As can be observed the increase in the H^* parameter resulted in a considerable decrease in particle adsorption kinetics. This is why for H^* = 0.15 the kinetic curve characteristic for elongated sphe-

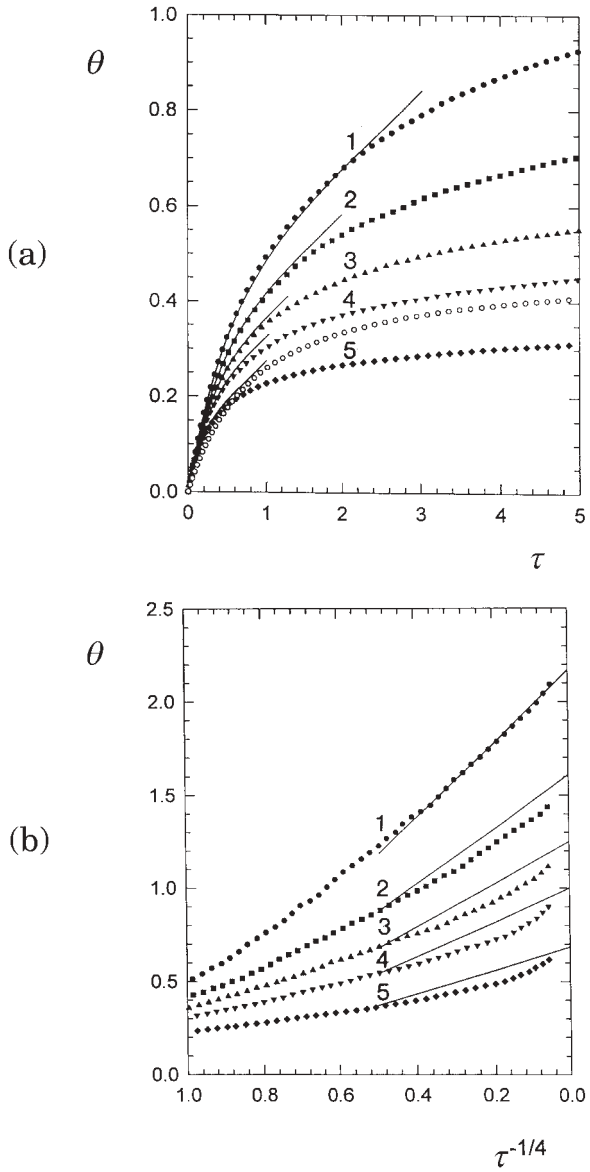

Figure 9. Part (a). Adsorption kinetics of interacting prolate spheroids ($A = 0.2$), the dependence of θ on τ for shorter times. The points denote numerical simulations performed for: (1) $H^* = 0$ (hard particles), (2) $H^* = 0.05$, (3) $H^* = 0.1$, (4) $H^* = 0.15$, (5) $H^* = 0.25$; the empty symbols denote the results obtained for hard spherical particles and the solid lines denote the analytical approximations calculated from Eqs. (19–20). Part (b). The dependence of θ on $\tau^{-1/4}$ determined numerically (points) for (1) $H^* = 0$ (hard particles), (2) $H^* = 0.05$, (3) $H^* = 0.1$, (4) $H^* = 0.15$, (5) $H^* = 0.25$; the solid lines show the analytical results calculated from Eq. (22) and Eq. (25).

roids become almost identical with the curve describing hard sphere adsorption (shown by open circles in Figure 9a). This may again lead to misinterpretations of experimental data because for a given ionic strength and particle size combination the hard sphere model can apparently reflect well adsorption kinetics of nonspherical particles. However, for lower ionic strength the differences would become significant.

On the other hand, the long-time limiting results shown in Figure 9b suggest that due to the appearance of interactions the jamming (maximum) coverages of interacting spheroidal particles θ_{mx} should be much smaller. Moreover, in contrast to hard particles, these coverages are not uniquely defined since they depend to a small extent on the maximum simulation time. However, for practical purposes, one can specify the following interpolation equation for the maximum coverages of interacting particles based on the effective hard particle concept[51]

$$\theta_{mx} = \theta_{\infty} \frac{C_1^0}{C_1^*} \tag{25}$$

where θ_{∞} is given by Eqs. (23–24), C_1^* by Eq. (14) and $C_1^0 = C_1^*(0)$.

Substituting Eq. (25) into Eq. (22) one obtains the linear fitting functions shown in Figure 9b. As can be seen some small positive deviations from the linearity occurred for interacting particles at longer times in accordance with previous results for the side-on adsorption[39]. This effect can in principle be accounted for by analyzing the target size and topology for the asymptotic regime close to jamming. We did not attempt to speculate further on this matter because the dimensionless adsorption times exceeding 10 are very difficult to attain in usual experiments involving proteins and colloids.[14]

The validity of the important from practical viewpoint Eq. (25) was checked[51] by performing extensive numerical simulations according to the above RSA scheme. The results obtained for prolate spheroids characterized by $A = 0.5$ and $A = 0.2$ are presented in Figure 10 together with the reference results for spheres ($A = 1$). The coordinate system $\theta_{mx} / \theta_{\infty}$ *vs.* κa was used in Figure 10 to make the effect of electrostatic interactions (described by Eq. (8)) more pronounced. It should be mentioned that the θ_{∞} values are of a primary interest in protein adsorption studies.[3–6,20–22] As can be seen in Figure 10 the approximate analytical estimations calculated from Eq. (25) are in a good agreement with the exact numerical simulations for a broad range of κa values, including the case characteristic for protein adsorption. Thus, the results shown in Figure 10 seem useful since they indicate that the concept of the effective interaction range is valid for surface coverages close to jamming. This provides one with an efficient method of estimating

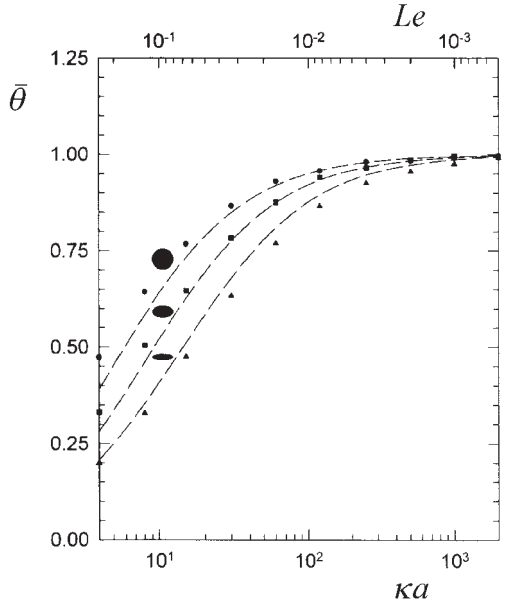

Figure 10. The dependence of the normalized maximum surface concentration $\bar{\theta} = \theta_{mx} / \theta_{\infty}$ on the κa parameter. The points denote the numerical results obtained for interacting prolate spheroids of various elongation, *i.e.*, $A = 1$ (spheres), $A = 0.5$ and $A = 0.2$; the broken lines denote the analytical approximations calculated from Eqs. (23, 25).

via Eq. (25) the jamming coverages for interacting particles of nonspherical shape.

It should also be mentioned that particle populations generated in RSA simulations, due to the relative simplicity of the algorithm, can be very large (*e.g.,* 10^4–10^5) assuring a good precision of the kinetic runs and jamming coverage estimations. These particle populations can also be exploited for determinig the structural characteristics of the monolayers like the pair correlation functions,[55] particle density fluctuations and directional order parameter.[56]

On the other hand, the RSA model, although very useful, has certain limitations due to neglecting the true 3D particle-interface interaction profile and the translational and rotational Brownian motion of adsorbing particles. It is expected that the former effect should decrease slightly particle adsorption for lower coverages (due to the energetically preferred side-on adsorption). However, the Brownian motion should probably compensate for this energetic affect so the net adsorption rate would be very similar to that predicted by the RSA model. At higher coverages, the particle/interface energetics should play a minor role since particle adsorption is largely deter-

mined by the topological constrains (adsorption may occur under orientations close to perpendicular only). The Brownian motion should play some role in modifying adsorption kinetics (analogously as in the case of spheres) but it is unlikely that the jamming coverages will be changed. These interaction and Brownian motion effects could in principle be considered by performing the Brownian Dynamics type simulations, analogously as for spheres.[19] However, at the present time such simulations for larger systems of nonspherical particles seem prohibitive.

The validity of the RSA approach for describing adsorption kinetics and structure of adsorbed monolayers has been confirmed experimentally in the case of spherical particles.[19,35,36,40] It has been demonstrated *inter alia* that the maximum surface coverages are decreased significantly[19] by decreasing the ionic strength (or particle size) in accordance with Eq. (25). By extrapolation, therefore, one can expect that the RSA model is applicable for nonspherical particles as well. However, due to difficulties in obtaining larger populations of monodisperse particles of nonspherical particles this hypothesis has not been verified yet.

CONCLUDING REMARKS

The theoretical analysis based on the RSA model showed that the surface blocking function $B(\theta)$ for nonspherical particles can well be approximated for not too high surface coverages by the polynomial expansion Eq. (10) from which the kinetic equations (Eqs. (18–20)) can be derived. Simulations performed according to the RSA scheme showed that these analytical expressions can be used for adsorption times $\tau < 2$. It has also been demonstrated that both adsorption rate and jamming coverages attained under the unoriended adsorption regime exceed considerably those predicted for the side-on adsorption regime.

The simulations revealed that the electrostatic interaction among adsorbing particles decrease to a considerable extent adsorption kinetics and jamming coverages for both adsorption regimes. This can be accounted for by introducing the effective hard particle concept with the effective interaction range proportional to the κa parameter, *i.e.*,

$$\frac{h^*}{a} = (\kappa a)^{-1} \xi$$

where the proportionality constant $\xi = (1/2) \ln (\phi_0 / \phi_{ch})$ is equal 3–4 for particle size around 0.1 μm.

By defining h^*/a, the maximum monolayer coverages of interacting spheroids particles can easily be calculated from Eqs. (13–14, 25) when the hard-particle values are known. Our theoretical predictions suggest, therefore, that the monolayer capacities of smaller colloid particles and proteins will be significantly decreased for low ionic strength of the suspensions.

It can also be deduced that due to compensation of some contradictory effects the results stemming from the RSA model discussed in our work will not be affected significantly when the particle/interface interactions and Brownian motion are considered.

Although no direct verification of these theoretical predictions has been carried out yet, the good agreement of the RSA model with experiments observed for spheres will suggest that the results presented in our work can be used as good estimates of adsorption processes of nonspherical particles.

REFERENCES

1. Z. Xia, L. Woo, and T. G. M. van de Ven, *Biorheology* **26** (1989) 359–375.
2. R. Bos, H. C. van der Mei, J. M. Meinders, and H. J. Busscher, *J. Microbiol. Methods* **20** (1994) 289–305.
3. J. Y. Yoon, H. Y. Park, J. H. Kim, and W. S. Kim, *J. Colloid Interface Sci.* **177** (1996) 613–620.
4. B. K. Lok, Yu-L. Cheng, and Ch. R. Robertson, *J. Colloid Interface Sci.* **91** (1983) 104–116
5. P. Schaaf, Ph. Dejardin, and A. Schmitt, *Langmuir* **3** (1988) 1128–1131, 1131–1135.
6. P. Schaaf and Ph. Dejardin, *Colloids Surf.* **31** (1988) 89–103.
7. N. C. Santos and M. A. R. B. Castanho, *Biophys. J.* **71** (1996) 1641–1650.
8. T. Sugimoto, *Adv. Colloid Interface Sci.* **28** (1987) 65–108.
9. J. J. Peters and G. Dezelić, *J. Colloid Interface Sci.* **50** (1975) 296–306.
10. E. Matijević, R. S. Sapieszko and J. B. Melville, *J. Colloid Interface Sci*. **50** (1975) 567–581.
11. E. Matijević and P. Schreiner, *J. Colloid Interface Sci.* **63** (1978) 509–524.
12. S. Hamada and E. Matijević, *J. Chem. Soc., Faraday Trans I* **78** (1982) 2147–2152.
13. D. M. Wilhelmy and E. Matijević, *Colloids Surf.* **16** (1985) 1–8.
14. M. Ozaki, S. Kratohvil, and E. Matijević, *J. Colloid Interface Sci.* **102** (1984) 146–151.
15. M. Ocana, M. Andres, M. Martinez, C. J. Serna, and E. Matijević, *J. Colloid Interface Sci.* **163**, (1994) 262.
16. C. C. Ho, A. Keller, J. A. Odell, and R. H. Otewill, *Colloid Polym. Sci.* **271** (1993) 469–479.
17. A. M. Wirenga and A. P. Philipse, *J. Colloid Interface Sci.* **180** (1996) 360–370.
18. I. Langmuir, in: C. G. Suits (Ed.), *The Collected Works of I. Langmuir*, 9, Pergamon Press, 1961, pp. 75–117.
19. Z. Adamczyk, B. Siwek, M. Zembala, and P. Belouschek, *Adv. Colloid Interface Sci.* **48** (1994) 151–280.
20. J. Feder and I. J. Giaever, *J. Colloid Interface Sci.* **78** (1980) 144–154.

21. B. R. Young, W. G. Pitt, and S. I. Cooper, *J. Colloid Interface Sci.* **124** (1988) 28–43.
22. J. D. Aptel, J. C. Voegel, and A. Schmitt, *Colloids Surf.* **29** (1988) 359–371.
23. B. Vincent, C. A. Young, and Th. F. Tadros, *J. Chem. Soc., Faraday Trans. I* **76** (1980) 665–673.
24. B. Vincent, M. Jafelicci, and P. F. Luckham, *J. Chem. Soc., Faraday Trans. I* **76** (1980) 674–682.
25. N. Kallay, M. Tomić, B. Biškup, I. Kunjašić, and E. Matijević, *Colloids Surf.* **28** (1985) 185–197.
26. T. Dąbrós and T. G. M. van de Ven, *Colloid Polymer Sci.* **261** (1983) 694–707.
27. T. Dąbrós and T. G. M. van de Ven, *J. Colloid Interface Sci.* **89** (1982) 232–244.
28. R. J. Gibbons, E. C. Moreno, and I. Etherden, *Infect. Immun.* **39** (1983) 280–289.
29. J. Sjollema, H. C. van der Mei, H. M. W. Vyen, and H. J. Busscher, *J. Adhesion Sci. Technol.* **4** (1990) 765–777.
30. B. Widom, *J. Chem. Phys.* **44** (1966) 3888–3894.
31. E. L. Hinrichsen, J. Feder, and T. Jossang, *J. Stat. Phys.* **11** (1986) 793–827.
32. P. Schaaf and J. Talbot, *J. Chem. Phys.* **91** (1989) 4401–4409.
33. P. Schaaf and J. Talbot, *Phys. Rev. Lett.* **62** (1989) 175–177.
34. J. W. Evans, *Rev. Modern Phys.* **65** (1993) 1281–1329.
35. Z. Adamczyk, M. Zembala, B. Siwek, and P. Warszyński, *J. Colloid Interface Sci.* **140** (1990) 123–137.
36. Z. Adamczyk, B. Siwek, and M. Zembala, *J. Colloid Interface Sci.* **151** (1992) 351–369.
37. L. R. White, *J. Colloid Interface Sci.* **95** (1983) 286–288.
38. Z. Adamczyk, P. Belouschek, and D. Lorenz, *Ber. Bunsenges. Phys. Chem.* **94** (1990) 1483–1492, *ibid* **94** (1990) 1492–1499, *ibid* **95** (1991) 566–573.
39. Z. Adamczyk and P. Weroński, *Langmuir* **11** (1995) 4400–4410.
40. Z. Adamczyk and P. Warszyński, *Adv. Colloid Interface Sci.* **63** (1996) 41–149.
41. R. Hogg, T. W. Healy, and D. W. Fuerstenau, *Trans. Faraday. Soc.* **62** (1966) 1638–1651.
42. P. Warszyński and Z. Adamczyk, *J. Colloid Interface Sci.* **187** (1997) 283–295.
43. G. M. Bell, S. Levine, and L. N. McCartney, *J. Colloid Interface Sci.* **33** (1970) 335–359.
44. J. A. Barker and D. Henderson, *J. Chem. Phys.* **47** (1967) 4714–4721.
45. L. Finegold and J. T. Donell, *Nature* **278** (1979) 443–445.
46. P. Viot and G. Tarjus, *Europhys. Lett.* **13** (1990) 295–300.
47. R. D. Vigil and R. M. Ziff, *J. Chem. Phys.* **91** (1989) 2599–2602.
48. S. M. Ricci, J. Talbot, G. Tarjus, and P. Viot, *J. Chem. Phys.* **97** (1992) 5219–5228.
49. J. Talbot, G. Tarjus, and P. Schaaf, *Phys. Rev A* **40** (1989) 4808–4811.
50. Z. Adamczyk and P. Weroński, *J. Chem. Phys.* **105** (1996) 5562–5573.
51. Z. Adamczyk and P. Weroński, *J. Colloid Interface Sci.* **189** (1997) 348–360.
52. T. Boublik, *Mol. Phys.* **29** (1975) 421–428.
53. J. Vieillard-Baron, *J. Chem. Phys.* **56** (1972) 4729–4744.
54. A. Tronin, T. Dubrovsky, and C. Nicoli, *Langmuir* **11** (1997) 385–389.
55. Z. Adamczyk and P. Weroński, *J. Chem. Phys.* **107** (1997) 3691–3697.
56. Z. Adamczyk and P. Weroński, *Bull. Pol. Acad. Sci., Chem.* **45** (1997) 419–430.

SAŽETAK

Adsorpcija nesferičnih čestica na međupovršini između čvrste i tekuće faze

Zbigniew Adamczyk i Paweł Weroński

Teorijski je analizirana lokalizirana adsorpcija nesferičnih čestica na međupovršini između čvrste i tekuće faze. Razmatran je približan model za izračunavanje međudjelovanja između čestica te između čestica i međupovršine. Pokazano je da se za konveksne čestice može rabiti Derjaguinov model, dok je za veće čestice znatno pogodniji pristup ekvivalentnih sfera. Energije izračunane na temelju analitičkih izraza navedenih modela rabljene su u numeričkim Monte-Carlo RSA *(random sequential adsorption)* simulacijama adsorpcije čestica. Prikazani su teorijski rezultati za blokirajuće parametre (uporabljive površinske funkcije) te za adsorpcijske kinetike izduženih i spljoštenih sferoida pri kratkim i dugim vremenima. Razmatrane su razlike između plošne (2D) i neorijentirane (kvazi-3D) adsorpcije čestica i specificirano je pravilo potencije za područja dugih vremena adsorpcije. Ekstrapolacijom kinetičkih rezultata određena je maksimalna pokrivenost za tvrde i interaktivne sferoide. Pokazano je, da je maksimalna pokrivenost za neorijentiranu adsorpciju izduženih objekata višestruko veća nego maksimalna pokrivenost za njihovu plošnu adsorpciju. Također je pokazano da odbojne interakcije dvostrukog sloja značajno smanjuju jednoslojni kapacitet adsorbiranih slojeva sferoidnih čestica. Razmatrane su posljedice tih fenomena na adsorpciju proteina.